

Lipophilic conjugates of methotrexate with short-chain alkylamino acids as DHFR inhibitors. Synthesis, biological evaluation, and molecular modeling

Rosario Pignatello,^{a,*} Salvatore Guccione,^a Stefano Forte,^b Claudia Di Giacomo,^d
Valeria Sorrenti,^d Luisa Vicari,^{e,†} Gloria Uccello Barretta,^c Federica Balzano^c
and Giovanni Puglisi^a

^aDipartimento di Scienze Farmaceutiche, Università degli Studi di Catania, Viale A. Doria 6, Città Universitaria, I-95125 Catania, Italy

^bDipartimento di Scienze Chimiche, Università di Catania, Viale A. Doria, 6, I-95125 Catania, Italy

^cDipartimento di Chimica e Chimica Industriale, Università degli Studi di Pisa, via Risorgimento 35, I-56126 Pisa, Italy

^dDipartimento di Chimica Biologica, Chimica Medica e Biologia Molecolare, Università di Catania, Viale A. Doria, 6, I-95125 Catania, Italy

^eDipartimento di Scienze Biomediche, Sezione di Patologia Generale, Università di Catania, via Androne, 86, I-95124 Catania, Italy

Received 21 November 2003; accepted 16 March 2004

Available online 22 April 2004

Abstract—Pursuing previous researches on lipophilic conjugates of methotrexate, aimed at over-crossing a form of transport resistance shown by some tumor cell lines toward the drug, a new series of derivatives is described in which the drug α - and γ -carboxyl groups have been linked through amide bonds to short-chain α -alkylamino acids (4–6 carbon atoms). A specific NMR study was performed to delineate the stereochemistry of the conjugates. The inhibitory activity of these compounds against the target enzyme, (bovine liver) dihydrofolate reductase, and a sensitive (CCRF-CEM) and a transport-resistant tumor cell subline (CEM-MTX) were assessed. The conjugates showed the ability of retaining the same inhibitory activity also against the resistant cell subline, against which the parent drug was much less active than against the wild one; the α,γ -bis(hexyl) derivative was the most active term of the series. Docking studies are in agreement with the proposed mode of interaction of these conjugates with the human DHFR.

© 2004 Elsevier Ltd. All rights reserved.

1. Introduction

Among the strategies proposed to enhance the passive internalization of drugs into cells, increasing their lipophilicity has been often demonstrated as a successful way. For instance, a similar problem arises with the antifolate drug methotrexate (4-amino-4-deoxy-*N*¹⁰-methylpteroyl-L-glutamic acid, MTX, **1**).^{1–3} MTX is widely used for the treatment of neoplastic diseases, such as non-Hodgkin's lymphoma, leukemia, choriocarcinoma, head and neck cancer, and osteogenic sarcoma, but also for some autoimmune diseases, for example, rheumatoid arthritis and psoriasis, and for the

prevention of graft-versus-host disease after transplantation. The development of different forms of drug resistance is a common limiting factor in the clinical efficacy of this agent. In particular, in man a form of *transport resistance* has been often observed, due to a defective efficiency of the active carrier system physiologically operating the cell internalization of reduced folates and MTX itself.⁴

Pursuing our previous research on lipophilic conjugates of MTX, in which the ability of long-chain 2-alkylamide or lipoamino acid (LAA) moieties in enhancing the passive uptake of the drug into resistant tumor cells was exploited,^{5–9} in the present work we have prepared and tested some lower homologues, in which the drug was conjugated through amide bonds to short-chain α -alkylamino acids (C-4–C-6). Conjugates were obtained as methyl esters and, upon hydrolysis, as the corresponding

* Corresponding author. Tel.: +39-095-7384021; fax: +39-095-222239; e-mail: r.pignatello@unict.it

† Present address: Istituto Oncologico del Mediterraneo (IOM Ricerca), via Penninazzo, 7, I-95030 Viagrande, Catania, Italy.

carboxylic acid sodium salts. The in vitro activity of the obtained compounds as inhibitors of the target enzyme dihydrofolate reductase (DHFR) and of the growth of sensitive as well as MTX-resistant tumor cell lines was estimated in comparison with the parent drug.

The conjugation of MTX with shorter-chain α -alkyl-amino acids is reasoned by the wish of increasing the lipophilicity of the drug, thus attaining its passive internalization into tumor cells, however without reducing dramatically the solubility of the resulting conjugates in aqueous media and biological environment, like often observed when drugs were conjugated to long-chain LAAs. In any case, the modification of the free carboxyl groups in the MTX glutamate residue would reduce the overall polarity of the drug and allow the penetration through cell membranes.³

We report here the synthesis and preliminary in vitro inhibitory activity evaluation of the synthesized conjugates against bovine liver DHFR (bDHFR), along with their cytotoxicity evaluation against one sensitive human lymphoblastoid cell line and a resistant subline (CCRF-CEM and CEM/MTX cells, respectively).

Docking studies, combined with a conformational NMR analysis of MTX conjugates in solution, were also carried out to gain insight into the structural properties of the complementary functional groups involved in the binding of the ligands to human DHFR (hDHFR), to rationalize whether the lipophilic side chain of the MTX conjugates only acts as a carrier, facilitating the passive uptake into cell cytoplasm, or might lead to an additional *valency* of the ligand,^{10–13} which results in an overall stabilization of the binding interactions, improving the affinity for the enzyme and/or the ADMET (Administration, Distribution, Metabolism, Excretion, Toxicity) properties.

2. Results and discussion

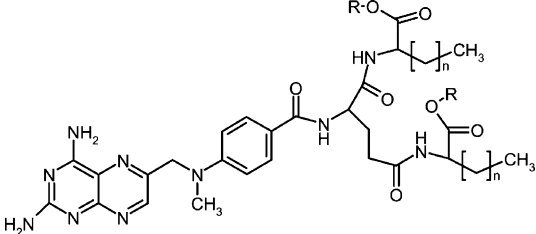
2.1. Chemistry

The synthesis of the short-chain α,γ -bis(2-alkylamino acid) conjugates of MTX **2a–4a** was afforded by means of a classical wet peptide synthesis procedure in dichloromethane and using a water-soluble carbodiimide (EDAC HCl), similarly to what described for other MTX-LAA conjugates previously described.^{6,8} Moreover, to verify the effect of molecule polarity on biological activity, the conversion of compounds **2a–4a** into the corresponding carboxylic acids **2b–4b** (as the sodium salts) was carried out by mild alkaline hydrolysis. Table 1 reports the structure and physico-chemical data of the two series of compounds.

The conjugates were obtained as their methyl ester with good yields and high purity. IR, mass, and ¹H NMR analyses confirmed the structure assigned to the compounds and sample homogeneity. In particular, in the IR spectra the appearance of the ester and amide bonds were visible, respectively, around 1730–1750 and 1680–1630 cm⁻¹ (data not shown), peaks not present in the spectrum of MTX; in the NMR analysis (Tables 2–4), the signals around 3.50–3.60 and 0.80 ppm further indicated the presence of the –COOCH₃ and the ω -methyl groups, respectively, introduced with the alkylamino acid moiety. Assuming a high enantiomeric purity of the used reagents (>98%), no racemization should occur.^{14,15}

The elemental analysis indicated that all the obtained conjugates are not anhydrous, even if kept for several hours under vacuum at 30 °C, but are solvated with 1/2–1 water molecule.

Table 1. Structure and calculated physico-chemical parameters of conjugates **2–4**

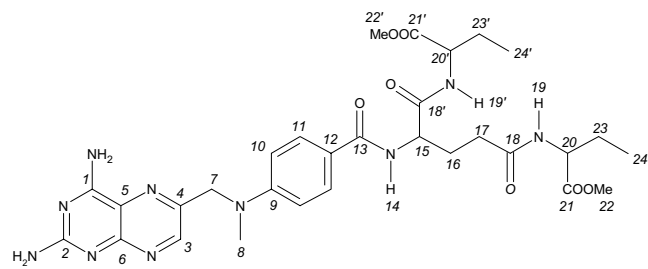


| Compound | R | n | CLog P ^a | CLog D _{7.4} ^b | Solubility (Log S) ^c |
|-----------|-----------------|---|---------------------|------------------------------------|---------------------------------|
| 2a | CH ₃ | 1 | 1.50 | 0.07 | -4.85 |
| 3a | CH ₃ | 2 | 2.56 | 0.90 | -5.39 |
| 4a | CH ₃ | 3 | 3.62 | 1.97 | -5.93 |
| 2b | Na | 1 | -1.134 | -6.51 | -4.60 |
| 3b | Na | 2 | -0.076 | -6.32 | -5.14 |
| 4b | Na | 3 | -0.982 | -5.20 | -5.68 |
| MTX | — | — | -0.28 | -6.02 | -3.77 |

^a ACD LogP, ver 5.15 (Advanced Chemistry Development Inc., Toronto, Canada).

^b Calculated apparent partition coefficient at pH 7.4 (Pallas 4.0 software, CompuDrug Chemistry Ltd, San Francisco, CA, USA).

^c Unit stripped algorithm (base 10) of the solubility measured in mol/L (Osiris Property Explorer, www.actelion.com).

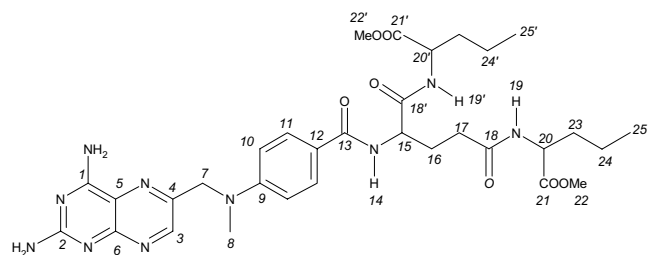
Table 2. ^1H (600 MHz, $\text{DMSO}-d_6$, 25 °C) and ^{13}C NMR (150 MHz, $\text{DMSO}-d_6$, 25 °C) chemical shifts (δ , ppm referred to TMS as external standard) of compound **2a**


| Atom | ^1H NMR δ (ppm) | ^{13}C NMR δ (ppm) |
|---------------|---------------------------------|--|
| NH_2 | 6.59, 7.64, 7.61 | |
| 3 | 8.55 | 149.14 |
| 7 | 4.77 | 54.58 |
| 8 | 3.20 | 39.15 |
| 10 | 6.81 | 111.02 |
| 11 | 7.71 | 128.88 |
| 14 | 8.07–7.94 | |
| 15 | 4.43 | 52.61, 52.73, 52.82, 52.99 |
| 19, 19' | 8.17 | |
| 20, 20' | 4.21–4.05 | 53.10, 53.22, 53.27, 53.30, 53.31 |
| 23, 23' | 1.78–1.45 | 24.15, 24.20, 24.22, 24.36 |
| 24, 24' | 0.90–0.74 | 10.11, 10.16, 10.22, 10.246, 10.253, 10.26 |
| 22, 22' | 3.63–3.54 | 51.62, 51.65, 51.73, 51.74, 51.76 |
| 16 | 2.04–1.80 | 27.50, 27.75 |
| 17 | 2.33–2.12 | 31.62, 31.70 |
| Quaternary C | | 121.16, 121.20, 121.22, 121.38, 145.98, 150.87, 155.16, 162.67, 162.82, 165.95, 166.01, 166.06, 166.10, 171.98, 172.04, 172.07, 172.13, 172.32, 172.34, 172.37, 172.40, 172.58, 172.61 |

2.2. NMR characterization of MTX conjugates

The conformational study was carried out on compound **4a**; in the lower homologue **2a** several conformers were present in the NMR spectrum, and no detailed conformational study was possible; compound **3a** showed a similar pattern than compound **4a**, suggesting an analogous conformation; however, minor components were individuated, maybe due to *syn/anti* type rotamers around the NHCO linkages.

The proton spectrum of **4a** in $\text{DMSO}-d_6$ (Fig. 1) is constituted by separate sets of signals spanning from 0.6 to 9.0 ppm. The signals have been attributed to the corresponding protons (Table 4) by 2D COSY and ROESY analyses. The spectral region between 0.6 and 2.4 ppm includes the resonances produced by methyl and methylene protons, with the exception of the methylene protons H-7, the *N*-methyl 8, and the two estereal methyls 22 and 22', producing, respectively, singlets at 4.56, 3.19, 3.56, and 3.58 ppm. The methine protons H-15, H-20, and H-20' are present between 4.10 and 4.50 ppm. In the high-frequency region, resonances

Table 3. ^1H (600 MHz, $\text{DMSO}-d_6$, 25 °C) and ^{13}C (150 MHz, $\text{DMSO}-d_6$, 25 °C) NMR characterization data of compound **3a**


| Atom | ^1H NMR δ (ppm) | ^{13}C NMR δ (ppm) |
|---------------|--|------------------------------------|
| 1, 2 | | 162.78, 162.62 |
| 3 | 8.55 (1H, s) | 149.09 |
| 4 | | 145.92 (H-3, H-7) |
| 5, 6 | | 121.22, 155.12 (H-3) |
| 7 | 4.77 (2H, s) | 54.79 |
| 8 | 3.20 (3H, s) | 39.06 |
| 9 | | 150.85 (H-7, H-8, H-11) |
| 10 | 6.81 (2H, d, $J = 8.9$ Hz) | 110.98 |
| 11 | 7.71 (2H, d, $J = 8.9$ Hz) | 128.81 |
| 12 | | 121.31 (H-10) |
| 13 | | 166.03 (H-11, H-14, H-15) |
| 14 | 8.02 (1H, d, $J = 7.5$ Hz) | |
| 15 | 4.41 (1H, ddd, $J = 7.5$ Hz, $J = 8.5$ Hz, $J = 4.9$ Hz) | 51.67 |
| 16 | 1.96 (1H, m), 1.86 (1H, m) | 27.44 |
| 17 | 2.22 (2H, m) | 32.86 |
| 18–18' | | 171.96 (H-17, H-19) |
| 19–19' | 8.17 (2H, d, $J = 7.5$ Hz), 8.15 (1H, d, $J = 7.5$ Hz) | |
| 20–20' | 4.21 (2H, m) | 51.57 |
| 21–21' | | 172.74, 172.51 (H-20, H-22) |
| 22–22' | 3.59 (3H, s), 3.57 (3H, s) | 51.50, 51.55 |
| 23–23' | 1.59 (1H, m), 1.60 (2H, m), 1.53 (1H, m) | 31.54 |
| 24–24' | 1.28 (8H, m) | 18.40 |
| 25–25' | | 18.47 |
| 26–26' | 0.84 (3H, t, $J = 7.0$ Hz), 0.82 (3H, t, $J = 7.0$ Hz) | 13.30, 13.35 |
| NH_2 | 7.62 (1H, br s), 7.41 (1H, br s), 6.58 (2H, br s) | |

arising from aromatic and amide or amine protons are found.

Among all the signals, the methyl and methylene protons of the two *n*-butyl chains are almost coincident, the two diastereotopic H-16a and H-16b protons, adjacent to the chiral carbon C-15, are well separate, whereas the two methylene protons H-17 are partially superimposed. As far as the amide protons are concerned, the NH-14 produces a well-resolved doublet at 8.03 ppm, whereas the two nuclei NH-19 and NH-19' generate completely superimposed doublets at 8.15 ppm. An anomalous signal pattern is originated by the two amine protons NH_2 -1 and NH_2 -2: among them one pair of protons produces coincident signals at 6.58 ppm, whereas the other amine protons originate two broad anisochronous signals at 7.63 and 7.40 ppm.

Information about the conformational features of the compound have been obtained both by detecting in the 2D ROESY maps the dipolar interactions originated by

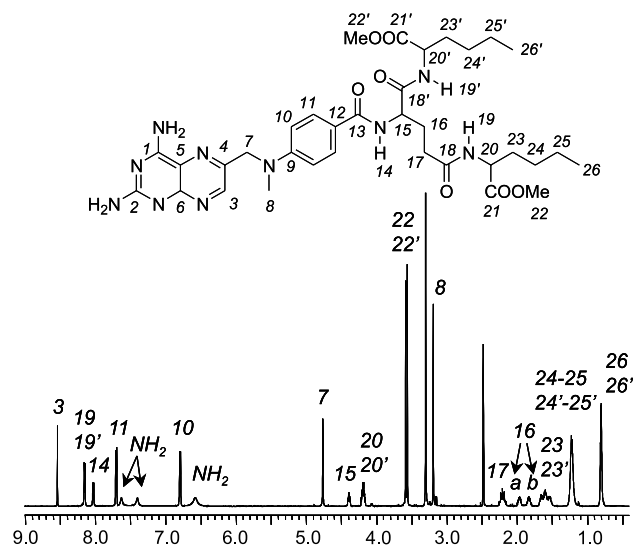
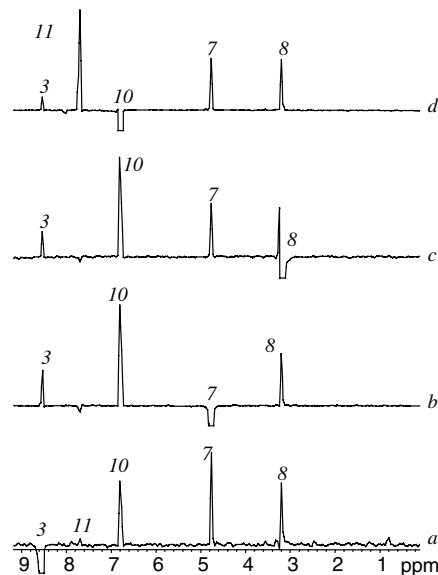
Table 4. ^1H (600 MHz, $\text{DMSO}-d_6$, 25 °C) and ^{13}C (150 MHz, $\text{DMSO}-d_6$, 25 °C) NMR characterization data of compound **4a**

| Atom | ^1H NMR δ (ppm) | ^{13}C NMR δ (ppm) ^a |
|-----------------|--|---|
| 1, 2 | | 162.82, 162.66 |
| 3 | 8.54 (1H, s) | 149.12 |
| 4 | | 145.96 (H-3, H-7) |
| 5, 6 | | 121.21, 155.17 (H-3) |
| 7 | 4.56 (2H, s) | 54.83 |
| 8 | 3.19 (3H, s) | 39.14 |
| 9 | | 150.85 (H-7, H-8, H-11) |
| 10 | 6.79 (2H, d, $J = 9.0$ Hz) | 111.00 |
| 11 | 7.70 (2H, d, $J = 9.0$ Hz) | 128.88 |
| 12 | | 121.37 (H-10) |
| 13 | | 166.09 (H-11, H-14, H-15) |
| 14 | 8.03 (1H, d, $J = 7.7$ Hz) | |
| 15 | 4.39 (1H, ddd, $J = 7.7$ Hz, $J = 9.1$ Hz, $J = 5.0$ Hz) | 52.56 |
| 16 | 1.96 (1H, m), 1.83 (1H, m) | 27.29 |
| 17 | 2.21 (2H, m) | 31.60 |
| 18–18' | | 172.00, 171.99 (H-17, H-19) |
| 19–19' | 8.15 (2H, d, $J = 7.5$ Hz) | |
| 20–20' | 4.20 (1H, m), 4.18 (1H, m) | 51.80 |
| 21–21' | | 172.81, 172.58 (H-20, H-22) |
| 22–22' | 3.58 (3H, s), 3.56 (3H, s) | 51.75, 51.66 |
| 23–23' | 1.66 (1H, m), 1.60 (2H, m), 1.53 (1H, m) | 30.54 |
| 24–24' | 1.23 (8H, m) | 21.42 |
| 25–25' | | 21.63, 21.66 |
| 26–26' | 0.81 (3H, t, $J = 7.0$ Hz), 0.80 (3H, t, $J = 7.0$ Hz) | 13.68 |
| NH ₂ | 7.63 (1H, s), 7.40 (1H, s), 6.58 (2H, s) | |

^a In parenthesis are reported the long range ^1H – ^{13}C correlations as detected by gHMBC.

protons in spatial proximity and by correlating the vicinal coupling constants of the NH–CH fragments to the corresponding dihedral angles.

Starting from the part of the molecule including the two aromatic moieties, we observed that the protons H-3, H-7, Me-8, and H-10 originate significant mutual inter-NOEs (Fig. 2); therefore these protons are all in close proximity. Furthermore, a dipolar interaction of the proton H-3 with the aromatic protons H-11 of the phenyl ring is detected (Fig. 2a). This effect, although small, clearly indicates that the two aromatic moieties belong to different planes leading the proton H-3 not only close to the aromatic protons H-10, but also to the protons H-11. The H-7 methylene (Fig. 2b) and the *N*-methyl group Me-8 protons (Fig. 2c), both giving the expected dipolar interactions with H-3 and H-10, must

**Figure 1.** ^1H NMR spectrum (600 MHz, $\text{DMSO}-d_6$, 25 °C) of compound **4a**.**Figure 2.** 2D ROESY analysis (600 MHz, $\text{DMSO}-d_6$, 25 °C, mix 0.3 s) of **4a**: traces corresponding to H-3 (a), H-7 (b), Me-8 (c), H-10 (d) protons.

be the first at the internal of the spatial region determined by the two aromatic groups and the latter also directed toward the H-3 proton rather than bent at the NH₂-1 protons.

On proceeding along the molecule toward the amino acidic fragments, we observed that the amide proton NH-14 (Fig. 3a) produces a very strong NOE on the aromatic protons H-11, whereas the effect on the adjacent methine proton H-15 is weaker, according to a conformational arrangement in which the NH-14 bond is mainly coplanar to the aromatic ring and transoid to its vicinal CH-15 bond. As a matter of fact the resolution of the Karplus equation correlating the observed vicinal coupling constant $^3J_{\text{NH14,CH15}}$ to the dihedral

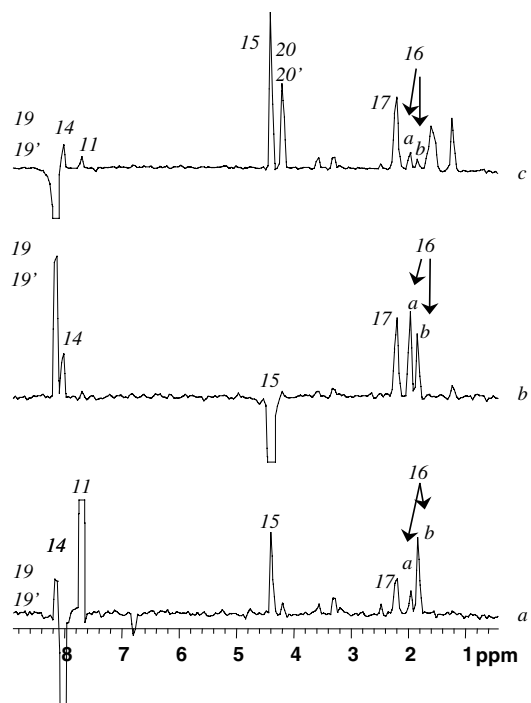


Figure 3. 2D ROESY analysis (600 MHz, DMSO- d_6 , 25 °C, mix 0.3 s) of **4a**: traces corresponding to NH-14 (a), H-15 (b), NH-19 and NH-19' (c) protons.

angle for this fragment affords the two solutions of 34° and 160°, the first of which can be excluded on the basis of the intensity of the dipolar interaction between the two involved protons compared to other detected NOEs, the latter one is according to the observed effects. The same NH-14 proton produces (Fig. 3a) low intensities NOEs on the diastereotopic protons H-16a and H-16b at 1.96 and 1.83 ppm, respectively, with the NH-14–H-16b effect more intense with respect to the NH-14–H-16a one. On the other hand, being the NH-14–H-16b effect comparable to that one NH-14–H-15 (Fig. 3a), we can also state that their corresponding interproton distances must be similar. The above conclusions are also supported by the analyses of the dihedral angles H-15–C-15–C-16–H-16a and H-15–C-15–C-16–H-16b, obtained on the basis of the two values of the vicinal couplings of 9.1 and 5.0 Hz. Among the possible solutions, the values of 29° and 140° are in optimal agreement with the observed NOE effects. Furthermore, the NH-14 proton originates a small NOE on the methylene protons H-17 (Fig. 3a), which could be transoid to the NH-14 bond and, hence, bent at the H-15 proton. Accordingly, in the trace of the 2D ROESY map corresponding to the H-15 proton a relevant dipolar interaction with the methylene protons H-17 is detected (Fig. 3b). All the other effects detected in this trace (Fig. 3b) are according to the above discussion; in fact the proton H-15 generates a NOE effect more intense on the proton H-16a (which is farther from NH-14) with respect to the effect originated on the proton H-16b (closer to NH-14). Therefore, the C–H-16b bond is transoid to the C–H-15 bond and cisoid to the N–H-14 one, whereas the reverse is true for C–H-16a.

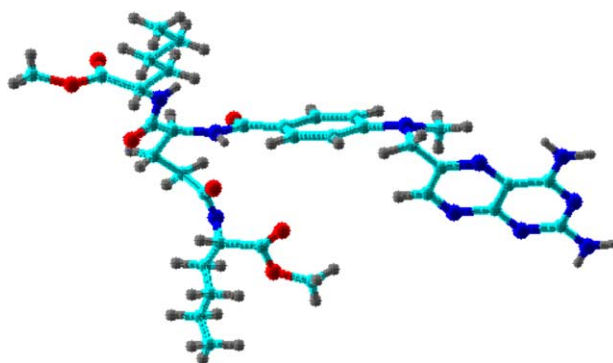


Figure 4. A graphical representation of the stereochemistry of **4a** in DMSO- d_6 as derived from the NOE data.

On the basis of the above data, among the dipolar interactions detected in the trace 'c' (Fig. 3) of the isochronous protons NH-19 and NH-19', the ones on H-15 and NH-14 can be attributed to NH-19', the effects on H-17 to NH-19 and the other NOEs could be attributed to both protons.

The proximity constraints imposed by the above discussed NOE data lead to the picture of Figure 4, where NH-14 could be involved in a hydrogen bond interaction with CO-18.

Relatively to the unusual behavior of the amine protons NH₂-1 and NH₂-2, no conclusions can be drawn, as any of them do not generate detectable dipolar interactions independently on the mixing time employed in the 2D ROESY measurements.

2.3. Evaluation of lipophilicity of conjugates 2–4

Table 1 reports the calculated physico-chemical properties of MTX and conjugates **2–4**, both in the ester and carboxylic form. Different computational softwares were used, depending on their performance, to calculate the partition coefficient (Log *P*), the distribution coefficient at a biological pH value (7.4, Log *D*), and the aqueous solubility (Log *S*).

In respect to MTX, the ester compounds **2a–4a** obviously showed a higher Log *P* value, proportional to the length of the side alkyl chain. Even the higher hexyl homologue **4a**, however, gave a Log *P* value (3.62) fully compatible with a pharmacological use, as compared with many available databases. At pH 7.4 (i.e., a pH value close to that one of media used for the biological studies), all the conjugates showed lower apparent partition coefficients (below 100), further underlining their 'drug-like' properties. Even at this pH value, compounds **2a–4a** displayed a higher lipophilicity that the parent MTX which, for its very polar features (a CLog *D*_{7.4} = −6.02 was given), has nearly no affinity for lipid domains of cell membranes. Therefore, the structure-related enhancement of the lipophilicity is coherent with an increase of cell membrane permeation for these conjugates.

When the carboxylic forms were evaluated, we observed for all the three compounds calculated $\text{Log } D_{7.4}$ values close to or lower than that one of MTX (between -5 and -6 log units), resulting from the introduction of two amino acid residues into the glutamate moiety of the drug. Such extremely high hydrophilicity in biological conditions explains why compounds **2b–4b** showed a lower inhibitory activity mainly against the MTX-resistant tumor cell, which would require a passive crossing of the cell membrane by the inhibitors.

Finally, all the compounds, in both forms, displayed a calculated aqueous solubility 1–2 orders lower than MTX, with no evident correlation to the ester or carboxylic state of the amino acid moieties. It must be however considered that even the starting MTX has a very low water solubility (a $\text{Log } S$ value of -4 is considered the minimum requirement for most drug; see www.organic-chemistry.org for further explanations).

2.4. In vitro biological evaluation

Basing of the starting idea of this work, we did not anticipate an increase of activity with respect to free MTX, but a differential activity profile than the parent drug against the two—sensitive and resistant—tested cell sublines. This would confirm the different pathway followed by MTX or its lipophilic conjugates in entering tumor cells. The biological results are presented in Figures 5–12 and summarized in Table 5, which gathers the relative IC_{50} values.

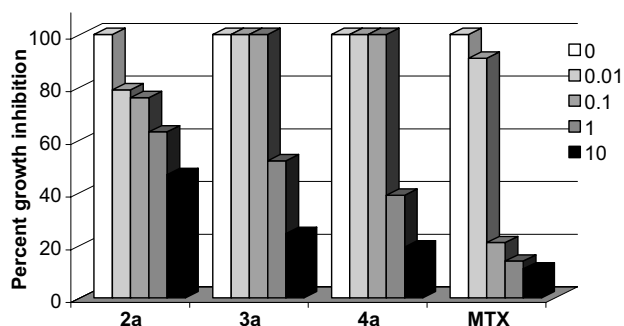


Figure 5. Growth inhibitory activity of ester conjugates **2a–4a** against wild CCRF/CEM cells (48-h incubation). Drug concentrations are given as micromolar.

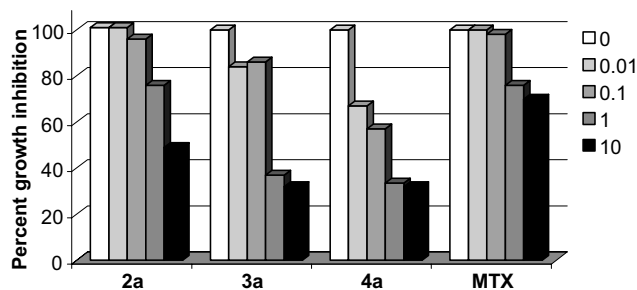


Figure 6. Growth inhibitory activity of ester conjugates **2a–4a** against CEM/MTX-resistant cells (24-h incubation). Drug concentrations are given as micromolar.

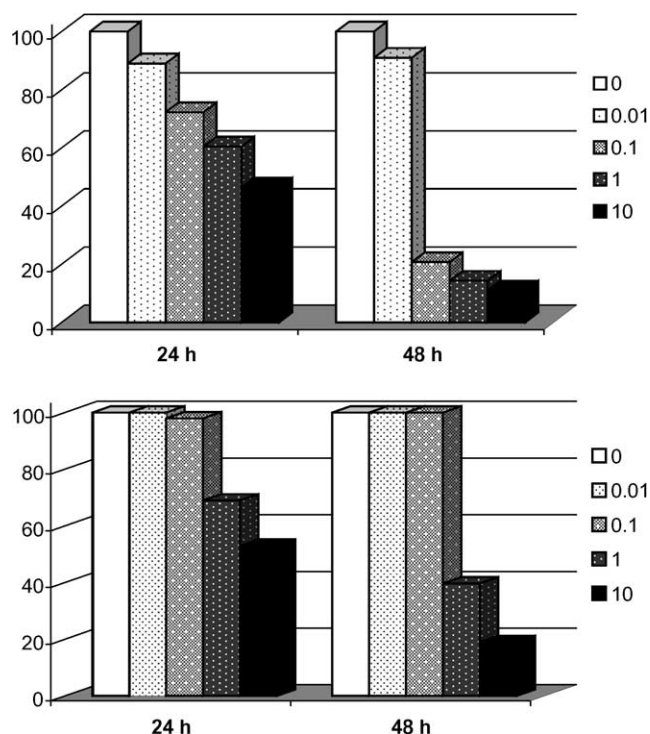


Figure 7. Time course of the inhibitory activity of MTX (top) and conjugate **4a** (bottom) against wild CCRF/CEM cells. Concentrations are expressed as micromolar.

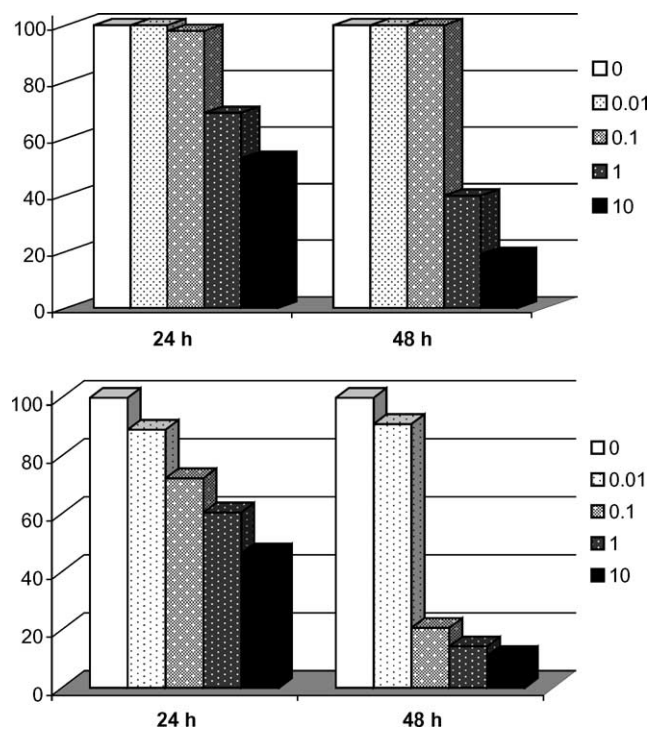


Figure 8. Time course of the inhibitory activity of MTX (top) and conjugate **4a** (bottom) against CEM/MTX-resistant cells. Concentrations are expressed as micromolar.

Actually, conjugates **2a–4a** still exerted a growth inhibitory activity against transport-resistant CEM/MTX cells, against which MTX is much less active. For

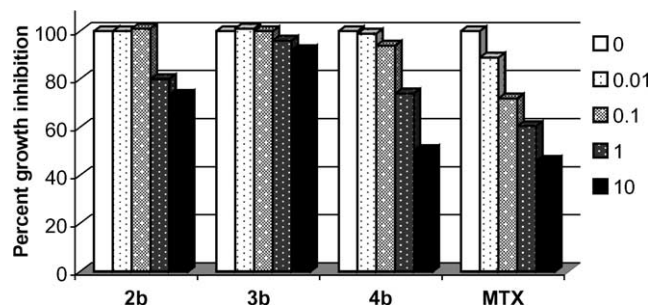


Figure 9. Growth inhibitory activity of acid conjugates **2b–4b** against wild CCRF/CEM cells (24-h incubation). Drug concentrations are given as micromolar.

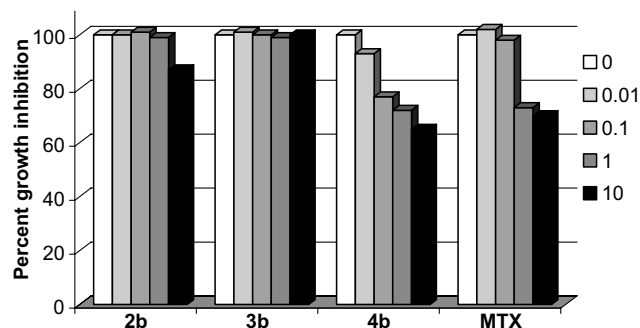


Figure 10. Growth inhibitory activity of acid conjugates **2b–4b** against CEM/MTX-resistant cells (24-h incubation). Drug concentrations are given as micromolar.

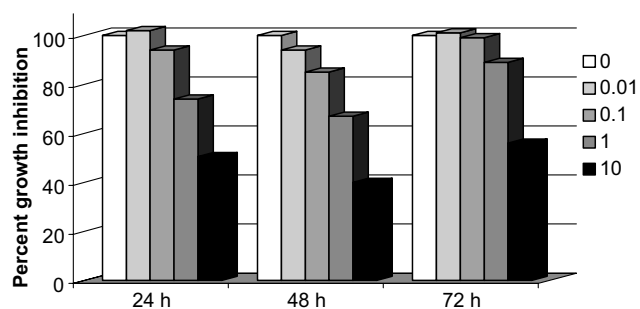


Figure 11. Time course of the inhibitory activity of conjugate **4b** against wild CCRF/CEM cells. Concentrations are expressed as micromolar.

instance, MTX showed a 79% and 86% inhibitory activity, at 0.1 M and 1 μ M concentrations, respectively, against the wild CCRF/CEM cell line (48-h incubation) (Fig. 5), while its activity was strongly reduced (12% and 4% cell growth inhibition, respectively) against the resistant subline (Fig. 6). Conversely, by observing in depth the activity profile of the most active among the prepared conjugates, the bis(hexyl) derivative **4a**, while displaying no significant activity at 0.1 μ M against the sensitive cells (Fig. 7), it exerted a 43% inhibition at the same concentration against the resistant subline (Fig. 8). Similarly, at 0.01 μ M compound **4a** gave a 33% inhibition against CEM/MTX cells, while MTX was unable to affect the cell growth (Fig. 8).

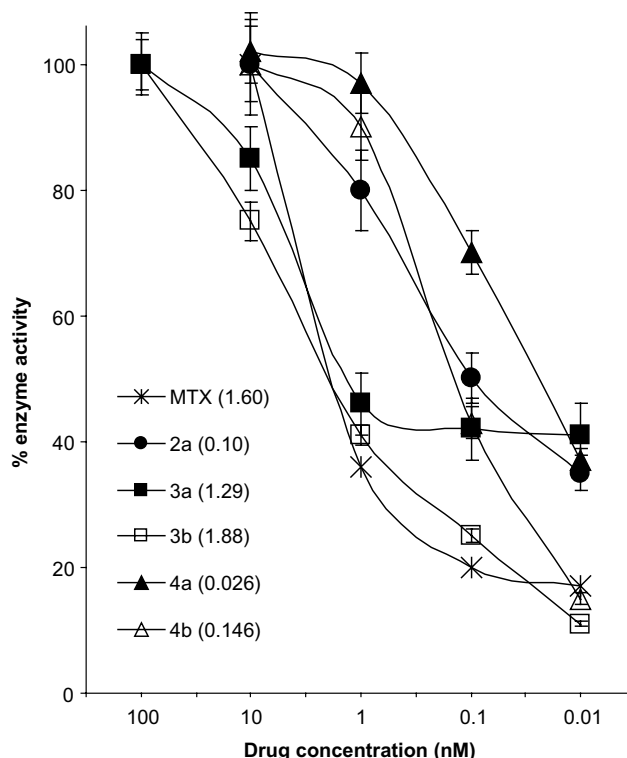


Figure 12. Inhibition pattern of bDHFR by MTX and conjugates **2–4**. IC₅₀ values (nM) are reported in paranthesis (the IC₅₀ values are indicative, since they were calculated basing on few experimental points).

Within the series of synthesized conjugates, the CEM/MTX cell growth inhibitory activity increased with a longer alkyl chain length, that is, in the order **4a** > **3a** > **2a**. Such a trend of cell growth inhibition versus the conjugates lipophilicity probably resulted from a balance between the actual concentrations of each compound at the two sides of cell membranes. It must be considered that their ability of penetrate passively through cell membranes can in the same time endorse their counter-extrusion back to the culture medium, a phenomenon that is only marginal for the parent MTX molecule which, upon polyglutamylaton, remains entrapped inside cells. Consequently, one possible explanation to the fact that the more lipophilic terms displayed the highest relative inhibitory activity, is the consequence of their ability to permeate the cell membrane and/or to cross the membrane back to the external medium, thus modifying the actual cellular concentration of the active compounds.

At higher drug concentrations (1 and 10 μ M), however, also conjugates **2a–4a** were active against the wild CCRF-CEM cells, suggesting a reduced affinity for the target enzymes but a residual inhibitory activity in these molecules, even after the conjugation of the parent drug with the alkylamino acid residues.

Another interesting reading of these data comes from comparing the inhibitory activity exerted at 24 or 48 h of drug incubation with the cell line (CCRF-CEM or

Table 5. Summary of inhibitory activity (IC_{50}) of conjugates **2–4** against CCRF-CEM and CEM/MTX cells (24-h incubation, except for marked samples)

| Compound | CCRF-CEM (μ M) | CEM/MTX (μ M) |
|-----------|---------------------------|--------------------|
| 2a | 6.10 ^a | 10.0 |
| 2b | >10 | >10 |
| 3a | 1.22 ^a | 0.84 |
| 3b | >10 | >10 |
| 4a | 0.25 ^a | 0.33 |
| 4b | 10.0 | >10 |
| MTX | 9.5 (0.045 ^a) | >10 |

^a 48-h incubation.

CEM/MTX cells for MTX and compound **4a**, respectively), against which they were more potent (Figs. 7 and 8). In fact, MTX showed a higher inhibitory activity after 48 h of incubation, as a result of the longer time needed to reach an equilibrium among the various steps (carrier-assisted cell uptake, active cell extrusion, polyglutamylation, etc.) that are known to regulate the actual intracellular MTX concentration. MTX is polyglutamylated over time, hence a time-dependent increase in inhibition with MTX is expected. Conversely, the lipophilic conjugate **4a** displayed no or less relationship with the time of permanence inside the cells, having a similar activity at both the incubation times, consistent with the cell entrance pathway (passive cell membrane penetration). Thus, perhaps these amide conjugates of MTX are less dependent on polyglutamylation to be active and/or retained in the cell.

When conjugates **2a–4a** underwent a mild hydrolysis, the corresponding alkylamino acids **2b–4b** were obtained (as the sodium salts). Such a modification change the polarity of the compounds and ultimately their mechanism of interaction with cell membrane structures. Compounds **2b–4b** showed a reduced growth inhibitory activity against both CCRF-CEM and CEM/MTX cell sublines, even for the most active term **4b** (Figs. 9 and 10), not far from that one of MTX. These data confirm that the polar carboxyl groups, like those ones present in the molecule of MTX, hinder the passive cross of cell membranes: these polar compounds would then require again an active carrier system to enter cells.

Furthermore, the lack of an increase of activity after 72 h of incubation (Fig. 11) suggests that the described amide conjugates did not undergo a hydrolytic cleavage of the amino acid group into the parent drug, and that the observed inhibitory activity must be ascribed to the whole conjugate molecules.

The inhibitory activity of conjugates **2–4** against bDHFR is outlined in Figure 12. All compounds showed a concentration-dependent inhibition of the enzyme, close to or higher than MTX, especially at lower concentrations (below 1 nM). The methyl esters **2a–4a** (Fig. 12, filled symbols) were more active against bDHFR than the corresponding acid forms (sodium salts) **3b** and **4b** (open symbols). In particular, the hexyl derivative compound **4a** showed 10-fold inhibitory activity than the carboxyl counterpart **4b**. Conjugate **3a** displayed a strange profile, with a lower inhibitory

activity at higher concentrations and a plateau at concentrations over 1 nM; this could be due to solubility problems, that reduced its true active concentration in the assay medium.

2.5. Molecular modeling studies

The relative differences observed in vitro between the ester derivatives and the carboxylic counterparts, negatively charged at pH 7.4, are in accordance with the docking studies (Figs. 13 and 14) performed by the software FLO+ (Version April03),^{16–18} showing the same trend of binding energies for all the ester derivatives compared to the corresponding carboxylic derivatives (e.g., $FreeE = -35.3$ kJ/mol for compound **4a** vs -37.4 for its carboxylate counterpart **4b**) and a similar binding mode (see below) inside the active site. Obviously electrostatics might be overemphasized because of missing solvent effects (solvation energy) certainly present, being the chains pointing to the bulky solvent. The slightly flipped carboxylate might force the γ -chain into a different conformation, leading to an additional interaction with a water molecule (Fig. 15), which cannot be related to a specific effect and does not justify any stabilizing effect by a water molecule. On the contrary, the strong additional hydrogen bond given by the NH group in the γ -side chain with Asp-21 (2.2) accounts at all for the better energy of interaction of the carboxylate compound **4b** compared to its ester counterpart **4a** (Fig. 14). This interaction cannot compensate for the decrease in lipophilicity due to the ester replacement, and the consequent reduced inhibitory activity observed on cell growth supports and *negatively validates* the working hypothesis.

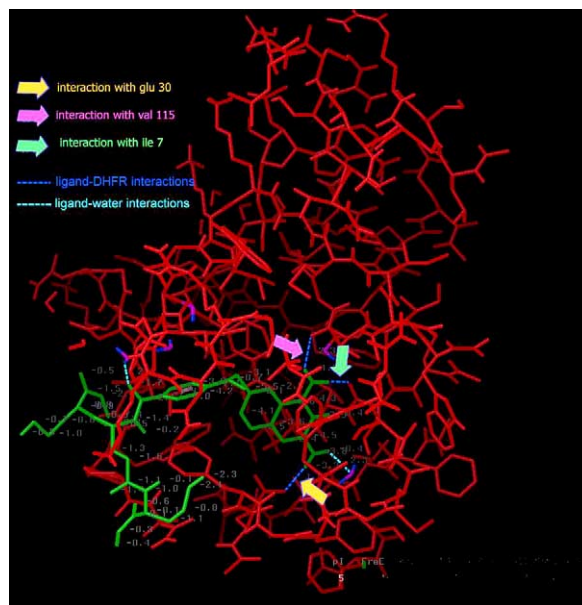


Figure 13. Docking (green sticks) of compound **4a** into hDHFR. Yellow, pink, and green arrows point to the interactions with Glu30, Val115, and Ile7. Ligand and water-mediated ligand interactions are displayed in blue and sky blue dotted lines, respectively. Compound **4b** showed a similar docking.

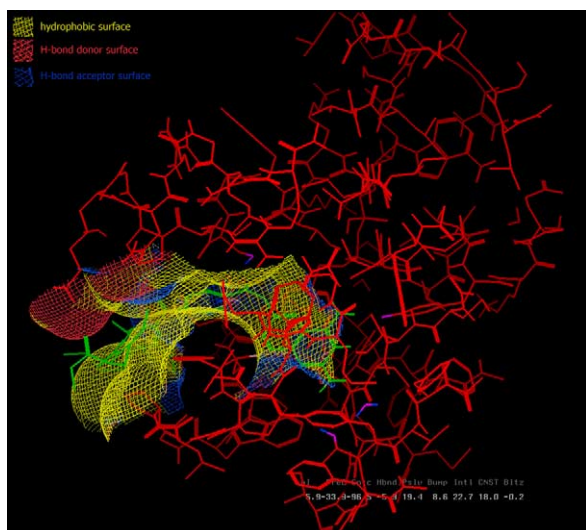


Figure 14. Surface mapping of hDHFR active site with compound **4a** docked (green sticks). Yellow mesh: hydrophobic; blue mesh: H-bond acceptor; red mesh: H-bond donor.

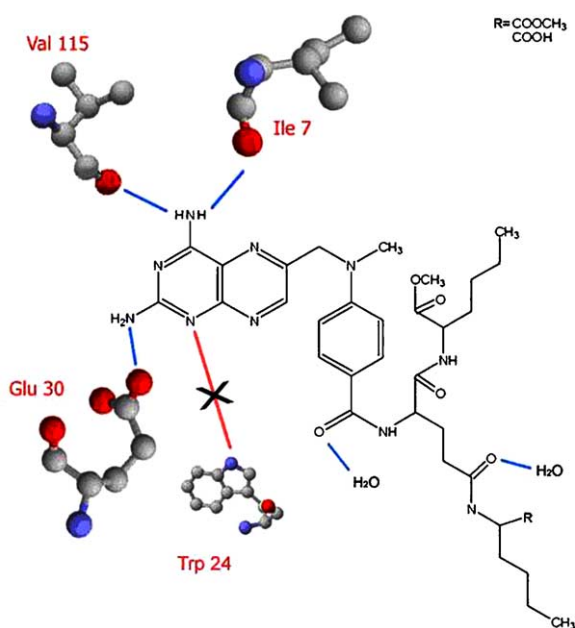


Figure 15. Schematic representation of interactions for compounds **4a** and **4b** into hDHFR.

The additional interaction is not a perturbing or vexing factor for binding to the active site, as also proved by the similar *in vitro* bDHFR inhibitory activity values observed. However, according to the initial hypothesis of this work, that the higher lipophilic character produced by the conjugation of MTX with LAAs positively affects the passive penetration of the drug into tumor cells, ultimately promoting its contact with the target enzyme,^{6,8,9} the NH 'hook', although a possible artifact due to the conformational uncertainty, might itself represent an aspect of the reduced lipophilicity, that is, of the stronger polar character of compound **4b**, that further worsens the passive cell entrance pathway.

According to a recently published crystallographic study by Borhani et al.²⁰ the 5-deazapteridine rings of all the inhibitors form identical contacts in the folate-binding site by hydrophobic and hydrogen-bond mediated interactions in a hydrophobic pocket (Fig. 14) adjacent to helix α B, with the 5-deazapteridine ring almost perpendicular to the amino acid side chain flipped approximately 180° along the ring long axis relative to the position of folate in the active site. Thus, the opposite side of the pteridine ring should be presented to the NADPH co-factor.¹⁹ Tight hydrogen bonds link the 5-deazapteridine ring to DHFR. The FLO+ graphic interface does not allow to display details concerned with the hydrophobic interactions. The mapped hydrophobic surface is displayed in Fig. 14. All the found interactions are in agreement with Klon et al.²⁰ (Figs. 13–15) except that between the deazapteridine N1 with GLU30 and some water mediated interactions.

Provided that these missing water interactions might arise from the penalty in the deleting of water (i.e., that ones forming less than three hydrogen bonds, as in Section 4) before the FLO+ docking, these hydration sites must be taken with caution. They might be artefacts in the crystallization process or might represent some kind of unspecific hydration effects by 'moving around' undefined surface waters.¹⁹ Only specific strongly preferred hydration sites are actually involved in the binding process.¹⁹

While the water mediated interaction between the amino group in N-2 is clearly displayed, that one at the N-8²⁰ can be easily recovered by manually adding a water molecules and repeating the docking. Noteworthy, manually adding the missing water bridges might recover all the interactions, as reported in the crystallographic study by Klon et al.,²⁰ leading to more stable complexes (about 1 kcal/mol more negative FreeE values), as a further evidence of the FLO+ (April03 version) capability.^{16–18} A strong interaction was found between the 2-amino group of the deazapteridine ring and the oxygen atoms of the Glu30 side chain, that is highly conserved in the active site of all vertebral DHFRs (Figs. 13 and 14). A second interaction between the N-1 and the Glu-30 side chain, leading to a double salt bridge²⁰ was not detected. The 4-amino group of the deazapteridine ring forms strong hydrogen bonds with Val115 and Ile7. The carboxylate group of Glu30 is substantially coplanar with the 5-deazapteridine rings of the inhibitors.

Since the 5-deazapteridine ring of all the inhibitors has the same structure and binds in nearly identical conformations to the active site, the lipophilic side chains, which do not access the active site 'volume' extending outside and are exposed to the bulky solvent, represent a moiety suitable for ADMET properties optimization, and regulates the alternative *no folate carrier*-mediated mechanism of cellular uptake without affecting the active site binding, or add *valency* to the ligands^{12–15} by properly located groups, which obviously must not affect negatively the lipophilic character of the molecule. Crystallographic studies are currently in progress.

```

DYS_HUMAN 1 VGS LNCIVAVSQNMIGKNGDLPWPPLRNEFRYFQRM TTTSSVEGKQNLVIMGKKTWFSI
DYS_BOVIN 1 V RPLNCIVAVSQNMIGKNGDLPWPPLRNE RQ YFQRM TTVSSVEGKQNLVIMGRKTWFSI
*****
DYS_HUMAN 61 PEKNRPLKGRINLVLSRELKEPPQGAHFLSRSLDDALKLTEQPELANKVDMVWVGGSSV
DYS_BOVIN 61 PEKNRPLK DRINIVLSRELKEPPKGAHFLAKSLDDAL ELIQDPEL TNKVDVWVWVGGSSV
*****
DYS_HUMAN 121 YKEAMNHHPGHLKLFVTRIMQDFESDTFFPEIDLEKYKLLPEYPGVLSDVQEEKGIKYKFE
DYS_BOVIN 121 YKEAMNKPGH VRLFVTRIMQEFESDAFFPEID FEKYKLLPEYPGV PLDVQEEKGIKYKFE
*****

```

Figure 16. Sequence alignment for human/bovine DHFR; 88.6% identity in 186 residues overlap. Score: 863.0; gap frequency: 0.0%.^{21–25}

Many literature reports showed the negative effects on DHFR affinity due to the substitution on MTX glutamate carboxyl groups, mainly that one in α -position.³ Our biological data indicated that using short-chain alkylamino acids did not reduce the affinity of the drug toward its target enzyme, in contrast with the reduced inhibitory activity observed for MTX conjugates with longer-chained LAA, previously described.⁶

The results presented provide detailed structural information on how these particular inhibitors bind to hDHFR. Therefore, an explanation can be made regarding the nature of the binding to bDHFR and, by extension, to hDHFR.

All of the amino acids changes between these two enzymes lie away from the active site, and would likely have minimal impact upon the binding of inhibitors. The bovine enzyme is then a suitable surrogate for the human form (Fig. 16).^{22–27}

Combining the NMR study with molecular modeling²¹ allowed also to gain a dynamic view of the binding process, that is, how protein and ligand affect each other after the binding occurs, supporting an induced-fit process. Superposition of the docked FLO conformation with the NMR one (Fig. 17) shows that the side chains are differently located. Provided that differences may arise from the different nature and inherent drawbacks of the two approaches, the solvent effects might affect the spatial disposition, by considering the polarizable groups present in the side chain (amides) and the solvent (sulfone).²¹

The increased puckering in the FLO-docked conformation may be due to the formation of favorable contacts with the amino acid residues of the highly hydrophobic DHFR active site (Fig. 14).²⁰

3. Conclusions

In this study we have integrated and negatively validated by a new series of conjugates the *dynamics* of a previously described series of lipophilic derivatives of MTX with long-chain lipoamino acids, using short-chained 2-alkyl- α -amino acid promoieties. The reduction of the alkyl chain length, while still improving the lipophilicity of the drug, impaired less the water solubility of the resulting conjugates. The chemical intervention at the level of the glutamate end of MTX molecule maintained a good affinity toward the target enzyme DHFR, as

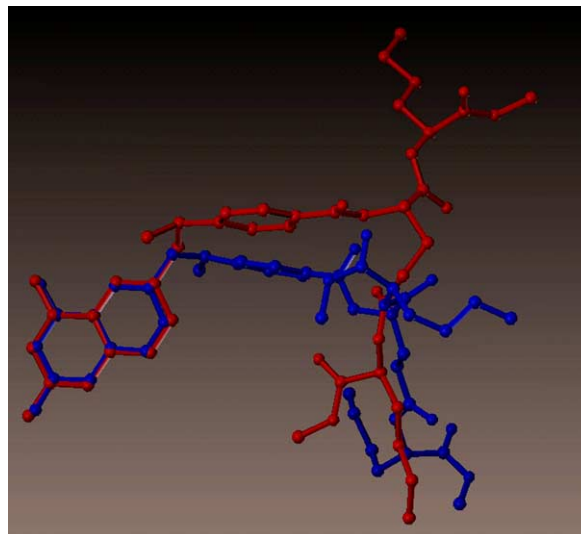


Figure 17. Superposition (ball and stick) of the docked FLO conformation (blue) with the NMR-established conformation (red) of compound **4a** (see Section 4 for details). Compound **4b** showed a similar behavior.

confirmed also by molecular modeling studies using FLO+. This was especially shown by the most active term, the hexyl derivate **4a**, further supporting the role of the side chains as an ADMET improvement moiety.

The comparison of the *in vitro* biological activity shown by these conjugates with respect to the longer homologues previously described,⁶ indicated for derivatives **2a–4a** a slight reduced activity against the sensitive tumor cell line CCRF-CEM, but a higher activity against the resistant CCRF/MTX subline.

These results let to presume that, despite the length of the alkyl side chain in the LAA residue, the substitution at the level of carboxyl functions on its own accounts for the differential profile of inhibition observed against the two tested cell lines, thus confirming the initial working hypothesis. Beyond possible nonspecific (e.g., van der Waals) interactions, the lipophilic side chains do not play a role as pharmacophores, whereas they are the determinants of the no carrier mediate uptake inside cell cytoplasm.

In conclusion, these conjugates could represent a good agreement between the need of increasing the lipophilicity of MTX molecule, to enhance its passive entrance into tumor cells, and keeping a certain solubility in water and, above all, maintaining the mechanism of biological activity.

The therapeutic association of MTX with one of its lipophilic derivatives may prevent the development of transport resistance to the drug, which has been often observed during clinical use of MTX. Moreover, similarly to the longer homologues previously described,^{6,8,9} these lipophilic conjugates would not be expected to form γ -polyglutamates once they enter cells, unlike the parent drug. This property has potential therapeutic

implications for the treatment of some MTX-resistant tumors whose resistance may be associated with a lower than normal capacity to form γ -polyglutamates, in comparison with highly proliferative tissues such as intestinal mucosa or marrow.^{28,29}

The therapeutic usefulness of this kind of MTX derivatives should furthermore be confuted in specific pathological situations, like HIV-correlated parasitic infections, where the responsible organisms (e.g., *Pneumocystis*, *Toxoplasma*, or *Leishmania*) do not possess active carriers for the uptake of folates, while being sensitive to DHFR inhibitors.^{30,31} To verify this latter hypothesis, work is in progress to determine the inhibitory activity of the MTX lipophilic conjugates described in the presents, as well as in out previous studies, against DHFR enzymes of human or different sources.

4. Experimental

4.1. General

IR spectra were recorded in KBr disks on a Perkin–Elmer 1600 series FTIR spectrophotometer. ¹H NMR were obtained in CDCl₃ or in 1:1 (v/v) CDCl₃/MeOD with a Brüker AM500 instrument at 500 MHz; chemical shifts are reported in ppm downfield from TMS as the internal reference. Mass spectra were recorded with a VG Analytical ZAB-SE instrument, using fast-atom bombardment (FAB) ionization. A 20-kV Cs⁺ ion bombardment was used, with 2 μ L of appropriate matrix (either 3-nitrobenzyl alcohol or thioglycerol/glycerol/TFA); a NaI methanol solution was added to produce nitrated species when no protonated molecular ions were observed. TLC was performed on Merck F₂₅₄₊₃₆₆ silica gel aluminum backed plates; spots were detected by UV light, exposure to iodine vapors or pouring into a 5% sulfuric acid ethanol solution. Column chromatography was carried out on Merck *dry* silica gel (230–400 mesh), with the eluent systems reported. Elemental analysis was carried out on a Carlo Erba mod. 1106 analyzer; samples were kept *in vacuum* for 24 h over P₂O₅ before analysis; found values are within ± 0.4 of theoretical ones.

4.2. Chemicals

MTX (purity > 98%, HPLC) was gifted by Wyeth SpA (Catania, Italy). Bovine liver DHFR (specific activity 7.8 U/mg protein), triethylamine (TEA) (Fluka), 1-ethyl-3-(3-dimethylaminopropyl)carbodiimide hydrochloride (EDAC HCl) (Aldrich), dihydrofolic acid, methyl D,L- α -aminobutyrate hydrochloride, and 1-hydroxybenzotriazole hydrate (HO-Bt) (Sigma), were purchased from Sigma–Aldrich Chimica Srl, Milan, Italy. The hydrochlorides of L-norleucin and L-norvalin methyl esters were purchased from Bachem AG (Bubendorf, Switzerland). DMF was distilled and dried before use; all other solvents and reactants were reagent grade or better and did not need further purification.

4.3. Methyl 2-({N²-[4-[(2,4-diaminopteridin-6-yl)methyl](methyl)amino]benzoyl}-N¹-[1-(methoxycarbonyl)propyl]- α -glutaminy]amino)butanoate (2a) (Table 1)

MTX (1 mmol), HO-Bt (2 mmol), and TEA (2 mmol) were dissolved in a dichloromethane/anhydrous dimethylformamide mixture (10:1 v/v, 10 mL). The resulting solution was added to 3 mmol of EDAC HCl and the mixture was stirred for 30 min in an ice-water bath at 0 °C; 2 mmol of the wished LAA methyl ester were then added and the mixture was further stirred at 0 °C for 2 h and thereafter at room temperature for about 24 h.

Solvents were then removed under vacuum and the solid dissolved in 40 mL of dichloromethane and consecutively extracted with 40-mL aliquots of a 5% aqueous acetic acid, brine, a 5% NaHCO₃ solution, and finally water. The organic phase was dried over sodium sulfate, filtered, and evaporated to dryness in vacuum. The product was finally purified by a column chromatography using a dichloromethane/methanol mixture gradient (from 97:3 to 9:1, v/v).

Yield: 75%, yellow crystals. *R*_f (dichloromethane–methanol, 9:1): 0.218; elemental analysis: found % (calculated for 1/2 H₂O): C, 54.53 (54.40); H, 6.36 (6.24); N, 21.38 (21.17); IR (cm⁻¹): 3347, 2963, 1740, 1615, 1207; FAB-MS (*m/z*): 653.6 [M+1]⁺ (100%), 653.6 (85%).

The higher homologues **3** and **4** were obtained in a similar fashion.

4.4. Methyl 2-({N²-[4-[(2,4-diaminopteridin-6-yl)methyl](methyl)amino]benzoyl}-N¹-[1-(methoxycarbonyl)butyl]- α -glutaminy]amino)pentanoate (3a)

Yield: 81%, yellow crystals. *R*_f (dichloromethane–methanol, 9:1): 0.224; elemental analysis: found % (calculated for 1/2 H₂O): C, 55.47 (55.72); H, 6.88 (6.57); N, 19.98 (20.30); IR (cm⁻¹): 3421, 2927, 1728, 1640, 1205; FAB-MS (*m/z*): 681.6 [M+1]⁺ (99%), 682.6 (4%).

4.5. Methyl 2-({N²-[4-[(2,4-diaminopteridin-6-yl)methyl](methyl)amino]benzoyl}-N¹-[1-(methoxycarbonyl)pentyl]- α -glutaminy]amino)hexanoate (4a)

Yield: 78%, yellow crystals. *R*_f (dichloromethane–methanol, 9:1): 0.236; elemental analysis: found % (calculated for 1/2 H₂O): C, 56.56 (56.80); H, 7.82 (7.57); N, 19.21 (19.50); IR (cm⁻¹): 3326, 2955, 1734, 1610, 1207; FAB-MS (*m/z*): 709.6 [M+1]⁺ (100%), 710.6 (23%).

4.6. Hydrolysis to the corresponding alkanolic acid sodium salts 2b–4b (Table 1)

Compounds **2a–4a** were dissolved in methanol and 2 equiv of a 1 N sodium hydroxide solution in a

methanol/water (4:1, v/v) mixture were added. The reaction mixture was gently stirred at a maximum temperature of 40 °C for some minutes, until TLC analysis showed the complete disappearance of the starting ester. The volatiles were then evaporated off in vacuum and the aqueous residue were washed with dichloromethane and freeze-dried (Edward Modulyo apparatus) to obtain a yellow solid. The structure of the obtained compounds was confirmed by IR analysis, checking the disappearance of the ester C=O signal, and mass spectra.

4.7. 2-[(N¹-(1-Carboxypropyl)-N²-{4-[(2,4-diaminopteridin-6-yl)methyl](methyl)amino}benzoyl}-α-glutaminy]aminobutanoic acid, sodium salt (2b)

Yield: 88%, yellow powder. Elemental analysis: found % (calculated for C₂₈H₃₄N₁₀Na₂O₇): C, 50.59 (50.30); H, 5.00 (5.13); N, 21.12 (20.95); IR (cm⁻¹): 3390, 2964, 1710, 1606, 1451; FAB-MS (*m/z*): 668.24 [M]⁺ (93%), 669.24 (32%), 670.24 (100%).

4.8. 2-[(N¹-(1-Carboxybutyl)-N²-{4-[(2,4-diaminopteridin-6-yl)methyl](methyl)amino}benzoyl}-α-glutaminy]norvalinate sodium salt (3b)

Yield: 82%, yellow powder. Elemental analysis: found % (calculated for C₃₀H₃₈N₁₀Na₂O₇): C, 52.17 (51.72); H, 5.78 (5.50); N, 19.83 (20.11); IR (cm⁻¹): 3385, 2967, 1708, 1606, 1450; FAB-MS (*m/z*): 696.27 [M]⁺ (100%), 697.27 (21%), 698.27 (4%).

4.9. 2-[(N¹-(1-Carboxypentyl)-N²-{4-[(2,4-diaminopteridin-6-yl)methyl](methyl)amino}benzoyl}-α-glutaminy]norleucinate sodium salt (4b)

Yield: 82%, yellow powder. Elemental analysis: found % (calculated for C₃₂H₄₂N₁₀Na₂O₇): C, 53.46 (53.03); H, 6.12 (5.84); N, 19.55 (19.33); IR (cm⁻¹): 3421, 2957, 1705, 1607, 1449; FAB-MS (*m/z*): 724.3 [M]⁺ (100%), 725.3 (43%), 726.3 (2%).

4.10. Calculation of physico-chemical properties

The relative lipophilicity of conjugates **2–4** was compared by calculating the partition coefficient (ACD LogP software, version 5.15; Advanced Chemistry Development Inc., Toronto, Canada), the distribution coefficient (Log *D*_{7.4}; Pallas 4.0 package, CompuDrug Chemistry Ltd, South San Francisco, CA, USA), and the aqueous solubility (Log *S*; Osiris Property Explorer, at www.actelion.com) (Table 1).

4.11. NMR studies

All NMR spectra in DMSO-*d*₆ were recorded on a Varian INOVA 600 spectrometer operating at 150 and 600 MHz for ¹³C and ¹H, respectively, using a 5 mm broadband inverse probe with *z*-axis gradient. The sample temperature was maintained at 25 °C. The 2D NMR spectra were obtained by using standard sequences. Proton gCOSY 2D spectra were recorded in

the absolute mode acquiring eight scans with a 3 s relaxation delay between acquisitions for each of 512 FIDs. The ROESY (rotating-frame Overhauser enhancement spectroscopy) spectra were recorded in the phase-sensitive mode, by employing a mixing time ranging from 0.05 to 0.8 s. The spectral width used was the minimum required in both dimensions. The pulse delay was maintained at 6 s; 256 hypercomplex increments of four scans and 2K data points each were collected. The data matrix was zero-filled to 2K × 1K and a sinebell function was applied for processing in both dimensions. The gradient gHSQC (heteronuclear single quantum coherence) experiment was recorded by employing the minimum spectral width in both F1 and F2 dimensions, a relaxation delay of 1 s, 128 increments of 128 scans and 2K data points. The gradient HMBC (heteronuclear multiple bond correlation) experiment was optimized for a long-range ¹H–¹³C coupling constant of 8 Hz. Spectrum was acquired with 128 time increments, 128 scans per *t*₁ increment, and a 3.6 ms delay period for suppression of one-bond correlation signals. The spectrum was acquired using no decoupling during acquisition. Tables 2–4 compare the NMR data for the conjugates **2a–4a**.

4.12. Cell growth inhibition tests

The human T-lymphoblastic leukemia cell line CCRF-CEM³² and an MTX-resistant (transport-defective) cell line (CEM/MTX)^{1,33} were grown at 37 °C, in a 5% CO₂ atmosphere in RPMI 1640 (HyClone), supplemented with 10% fetal calf serum, glutamine (2 mM), and antibiotics. Cells were plated in plastic 24-well plates at a concentration of 1 × 10⁵ cells/mL/well and test compounds were concomitantly added in a concentration range of 0.01–10 μM. Dilutions were made using the culture medium from 1 mM stock solutions of the drugs in anhydrous DMSO. Controls were treated with an equivalent amount of solvent, diluted as above, to assess the absence of toxicity due to the solvent.

After 24–72 h of incubation viable cells were counted with a haemocytometer by trypan blue exclusion assay. All the experiments were repeated three times in duplicate. Cell growth inhibition was plotted versus drug concentration (Figs. 5–11); IC₅₀ data are summarized in Table 5.

4.13. DHFR inhibition assay

Drug effect on bDHFR activity was measured by following NADPH oxidation at λ = 340 nm.⁵ The assay mixture contained 1 M sodium acetate buffer (pH 6.0), 0.6 M KCl, 50 μM NADPH, 50 μL DMSO (control) or the same volume of a DMSO solution of test compounds, to a final concentration ranging between 10⁻⁵ and 10⁻¹¹ M, and 0.02 units of BDHFR, in a final volume of 3 mL. After enzyme addition, the mixture was incubated at 23 °C for 5 min; the reaction was started by adding 33 μM dihydrofolic acid. The change in absorbance at λ = 340 nm (Δ_{abs340}) was followed for 10 min,

during which the activity was linear with respect to time. Results are reported as percent inhibition of the enzyme activity versus control (Fig. 12); each value is the mean \pm SD of six experiments. IC₅₀ values have also been reported with only an indicative significance, basing on the few number of experimental points used.

4.14. Molecular modeling

The molecular modeling studies were carried on a SGI R5000 and OCTANE R12000 workstation operating under IRIX 6.5.+ using the software FLO+ (version April03), a 'multifunctional' molecular design program, which uses an Amber/MM2 force field.^{16–18} FLO+ is a program for (i) database screening using docking to a binding site and potency scoring; (ii) reliable docking for drug design and QSAR (quantitative structure activity relationships) applications. A program (QXP+) can distribute jobs on multiprocessors and over networks including LINUX clusters.

A family of new near systematic dockers (zipdockers) are capable of fast docking for database screening and of slower very thorough docking for evaluation of potency and binding mode. A relative potency scoring function, based on the analysis of a number of computer docked SAR series, predicts X-ray docking modes and relative potency. The function used ensembles of docking modes and is called BSCORE (Boltzmann scoring). A potency prediction method called CONTACT predicts relative potencies.^{16–18}

Part of FLO+ is also a QSAR tool to develop specific scoring functions for individual series of docked structures of known potency. The new scoring function is based on the general scoring function, which is tuned using constraints to minimize changes in the coefficients.

Structures were built by the building option in FLO+ (version April03) with a R,S,S, configuration. The used synthetic procedure did not led to changes in chirality in respect to the starting reagents.^{10,11} Docking studies were carried out by the QXP fulldock+ module (1000 and 3000 cycles) using the hDHFR structure as in the Brookhaven Protein Databank (.pdb codes 1KMS and 1KMV). No qualitative changes were observed in the ligand position at 1000 and 3000 cycles. Slight changes in the interaction energies were observed at 3000 cycles. Reported energy values refer to 3000 cycles dockings. The coordinates of each pdb file were carefully checked and the co-crystallized ligand extracted. In order to mimic a more real situation, the NADPH co-factor was not deleted.³⁴ Actually, deleting the co-factor did not change the docking but produced a less stable (higher energy) complex according to its stabilizing role. The water molecules were deleted except of those ones forming three hydrogen bonds with the active site residues. The atom potential types bond orders were carefully checked to evaluate their correctness with respect to the intended structure. According to 'computational titration' data by the software HINT^{35–37} (data not shown) as in SYBYL 6.8, the azapteridine ring was

considered as charged, that is, protonated in N-1^{2038–41}, whereas the carboxylic group of derivatives **2b–4b** was considered in its dissociated form according to the pH (around 7) used for the biological assays. Contrary to Cannon and co-workers,^{34–37} also HINT scoring the *E. coli* DHFR showed the same trend (data not shown). The NMR solved structure of compound **4a** was exported to .pdb file by the PCMODEL software.⁴² The built structure was minimized to obtain proper bond lengths and angles, hence the atomic cartesian coordinates were adjusted according to the NMR ones. The atom potential types bond orders were carefully checked to evaluate their correctness with respect to the intended structure. The fit atom routine as in SYBYL 6.9³⁶ was used for the superposition (Fig. 17) between the FLO-docked^{16–18} (exported as .pdb) and NMR conformations.

Acknowledgements

This research was in part supported by the Italian Ministero dell'Istruzione e della Ricerca (MIUR) (Programma di ricerca COFIN 2002: Direzioneamento attivo e rilascio di farmaci antitumorali mediante sistemi colloidali e particellari).

Dr. Colin McMartin (Thistlesoft, Colebrook, CT 06021, USA) is gratefully acknowledged for the software FLO+ (version April03) and the valuable discussion he has provided. The authors are also grateful to Dr. David W. Borhani (Abbott Bioresearch Center, Worcester, MA 01605, USA); A. Héroux (Brookhaven National Laboratory, Upton, NY 11973, USA), and Professor S. F. Queener (Department of Pharmacology and Toxicology, Indiana University School of Medicine, Indianapolis, IN 46202, USA) for the thoughtful suggestions on DHFR. Thoughtful advices by Professor R. Menicagli (Dipartimento di Chimica e Chimica Industriale, Università degli Studi di Pisa, Pisa, Italy), and Professor A. Rescifina (Dipartimento di Scienze Chimiche, Università degli Studi di Catania, Catania, Italy) on the chirality assignment were appreciated.

References and notes

1. Rosowsky, A.; Lazarus, H.; Yuan, G. C.; Beltz, W. R.; Mangini, L.; Abelson, H. T.; Modest, E. J.; Frei, E., III. *Biochem. Pharmacol.* **1980**, *29*, 648–652.
2. Piper, J. R.; Montgomery, J. A.; Sirotinak, F. M.; Chello, P. L. *J. Med. Chem.* **1982**, *25*, 182–187.
3. Rahman, L. K. A.; Cchabra, S. R. *Med. Res. Rev.* **1988**, *8*, 95–156.
4. Moscow, J. A. *Leuk. Lymphoma* **1998**, *30*, 215–224.
5. Pignatello, R.; Sorrenti, V.; Spampinato, G.; Pecora, T.; Panico, A.; Di Giacomo, C.; Fresta, M.; Vanella, A.; Puglisi, G. *Anti-Cancer Drug Des.* **1996**, *11*, 253–264.
6. Pignatello, R.; Jansen, G.; Kathmann, I.; Puglisi, G.; Toth, I. *J. Pharm. Sci.* **1998**, *87*, 367–371.
7. Pignatello, R.; Spampinato, G.; Sorrenti, V.; Vicari, L.; Di Giacomo, C.; Vanella, A.; Puglisi, G. *Pharm. Pharmacol. Commun.* **1999**, *5*, 299–305.

8. Pignatello, R.; Spampinato, G.; Sorrenti, V.; Vicari, L.; Di Giacomo, C.; McGuire, J. J.; Russell, C. A.; Puglisi, G.; Toth, I. *Eur. J. Pharm. Sci.* **2000**, *10*, 237–245.
9. Pignatello, R.; Vicari, L.; Sorrenti, V.; Di Giacomo, C.; Spampinato, G.; Puglisi, G.; Toth, I. *Drug Dev. Res.* **2001**, *52*, 454–464.
10. Mammen, M.; Choi, S.-K.; Whitesides, G. M. *Angew. Chem.* **1998**, *110*, 2908–2953.
11. Mammen, M.; Choi, S.-K.; Whitesides, G. M. *Angew. Chem., Int. Ed.* **1998**, *37*, 2755–2794.
12. Germain, R. N. *Curr. Biol.* **1997**, *7R*, 640–644.
13. Metzger, H. J. *Immunol.* **1992**, *149*, 1477–1487.
14. Sheehan, J. C.; Hess, G. P. *J. Am. Chem. Soc.* **1955**, *77*, 1067–1068.
15. Sheehan, J. C.; Yang, D.-D. H. *J. Am. Chem. Soc.* **1958**, *80*, 1154–1158.
16. McMartin, C.; Bohacek, R. S. *J. Comput.-Aided Mol. Des.* **1997**, *11*, 333–344, and references cited therein.
17. QXP is the molecular mechanics module in FLO+ (version April03); a molecular design program commercially available from: Colin McMartin, Thistlesoft, PO Box 227, Colebrook, CT 06021, USA. A LINUX version of FLO+ will be shortly released.
18. Guccione, S.; Doweyko, A.; Chen, H. M.; Uccello Barretta, G.; Balzano, F. *J. Comput.-Aided Mol. Des.* **2000**, *14*, 647–657, and references cited therein.
19. Podjarny, A. D.; Howard, E. I.; Urzhumtsev, A.; Grigera, J. R. *Proteins: Struct. Funct. Genet.* **1997**, *28*, 303–312.
20. Klon, A. E.; Heroux, A.; Ross, L. J.; Pathak, V.; Johnson, C. A.; Piper, J. R.; Borhani, D. W. *J. Mol. Biol.* **2002**, *320*, 677–693.
21. Uccello-Barretta, G.; Balzano, F.; Sicoli, G.; Friglola, C.; Aldana, I.; Monge, A.; Paolino, D.; Guccione, S. *Bioorg. Med. Chem.* **2004**, *12*, 447–458.
22. Prendergast, N. J.; Delcamp, T. J.; Smith, P. L.; Freisheim, J. H. *Biochemistry* **1988**, *27*, 3664–3671.
23. Gasteiger, E.; Gattiker, A.; Hoogland, C.; Ivanyi, I.; Appel, R. D.; Bairoch, A. *Nucl. Acids Res.* **2003**, *31*, 3784–3788. Available from: <http://us.expasy.org>.
24. Lebrun, E.; Tu, Y. X.; van Rapenbusch, R.; Banijamali, A. R.; Foye, W. O. *Biochim. Biophys. Acta* **1990**, *1034*, 81–85.
25. Selinsky, B. S.; Perlman, M. E.; London, R. E.; Unkefer, C. J.; Mitchell, J.; Blakley, R. L. *Biochemistry* **1990**, *29*, 1290–1296.
26. Blakley, R. L.; Piper, J. R.; Maharaj, G.; Appleman, J. R.; Delcamp, T. J.; Freisheim, J. H.; Kulinski, R. F.; Montgomery, J. A. *Eur. J. Biochem.* **1991**, *196*, 271–280.
27. Wang, Y.; Bruenn, J. A.; Queener, S. F.; Cody, V. *Antimicrob. Agents Chemother.* **2001**, *45*, 2517–2523.
28. McCloskey, D. E.; McGuire, J. J.; Russell, C. A.; Rowan, B. G.; Bertino, J. R.; Pizzorno, G.; Mini, E. *J. Biol. Chem.* **1991**, *266*, 6181–6187.
29. McGuire, J. J. In *Anticancer Drug Development Guide: Antifolate Drugs in Cancer Therapy*; Jackman, A. L., Ed.; Humana: Totowa, 1998; pp 339–363.
30. Gangjee, A.; Yu, J.; McGuire, J. J.; Cody, V.; Galitsky, N.; Kisliuk, R. L.; Queener, S. F. *J. Med. Chem.* **2000**, *43*, 3837–3851.
31. El Fadili, A.; Richard, D.; Kundig, C.; Ouellette, M. *Biochem. Pharmacol.* **2003**, *66*, 999–1008.
32. Foley, G. F.; Lazarus, H.; Farber, S.; Uzman, B. G.; Boone, B. A.; McCarthy, R. E. *Cancer* **1965**, *18*, 522–529.
33. Westerhof, G. R.; Schornagel, J. H.; Kathmann, I.; Jackman, A. L.; Rosowsky, A.; Forsch, R. A.; Hynes, J. B.; Boyle, F. T.; Peters, G. J.; Pinedo, H. M.; Jansen, G. *Mol. Pharmacol.* **1995**, *48*, 459–471.
34. Cannon, W. R.; Garrison, B. J.; Benkovic, S. J. *J. Mol. Biol.* **1997**, *271*, 656–668.
35. Kellogg, G. E.; Abraham, D. J. *Eur. J. Med. Chem.* **2000**, *35*, 651–661. Available from: www.edusoft-lc.com.
36. Fornabaio, M.; Cozzini, P.; Mozzarelli, A.; Abraham, D. J.; Kellogg, G. E. *J. Med. Chem.* **2003**, *46*, 4487–4500, and references cited therein.
37. SYBYL Molecular Modelling Software, version 6.8 and 6.9; Tripos Inc.: 1699 S-Hanley Rd, Suite 303, St. Louis, MO 63144-2913, USA (www.tripos.com).
38. Cocco, L.; Groff, J. P.; Temple, C., Jr.; Montgomery, J. A.; London, R. E.; Matwiyoff, N. A.; Blakely, R. L. *Biochemistry* **1981**, *20*, 3972–3978.
39. Cocco, L.; Roth, B.; Temple, C., Jr.; Montgomery, J. A.; London, R. E.; Blakely, R. L. *Arch. Biochem. Biophys.* **1983**, *226*, 567–577.
40. London, R. E.; Howell, E. E.; Warren, M. S.; Kraut, J.; Blakely, R. L. *Biochemistry* **1986**, *25*, 7229–7235.
41. Andrews, P. R.; Craik, D. J.; Martin, J. L. *J. Med. Chem.* **1984**, *27*, 1648–1657.
42. PCMODEL, version 6 (1993–1996). Serena Software, Box 3076 Bloomington, IN 47402-3076, USA (www.serena-soft.com).